Magnitude of quantum effects in classical spin ices

Jeffrey G. Rau[1] and Michel J. P. Gingras[1,2,3,4,5]

[1]*Department of Physics and Astronomy, University of Waterloo, Ontario, N2L 3G1, Canada*

[2]*Perimeter Institute for Theoretical Physics, Waterloo, Ontario, N2L 2Y5, Canada*

[3]*Canadian Institute for Advanced Research, 180 Dundas Street West, Suite 1400, Toronto, ON, M5G 1Z8, Canada*

[4]*Quantum Matter Institute, University of British Columbia, Vancouver, BC, V6T 1Z4, Canada*

[5]*TRIUMF, Theory Group, 4004 Wesbrook Mall, Vancouver, BC V6T 2A3, Canada*

(Received 20 March 2015; revised manuscript received 11 September 2015; published 19 October 2015)

The pyrochlore spin ice compounds $Dy_2Ti_2O_7$ and $Ho_2Ti_2O_7$ are well described by classical Ising models down to low temperatures. Given the empirical success of this description, the question of the importance of quantum effects in these materials has been mostly ignored. We show that the common wisdom that the strictly Ising moments of isolated Dy^{3+} and Ho^{3+} ions imply Ising interactions is too naïve; a more complex argument is needed to explain the close agreement between theory and experiment. From a microscopic picture of the interactions in rare-earth oxides, we show that the high-rank multipolar interactions needed to induce quantum effects in these two materials are generated only very weakly by superexchange. Using this framework, we formulate an estimate of the scale of quantum effects in $Ho_2Ti_2O_7$ and $Dy_2Ti_2O_7$, finding it to be well below experimentally relevant temperatures. We discuss the implications of these results for realizing quantum spin ice in other materials.

DOI: 10.1103/PhysRevB.92.144417 PACS number(s): 75.10.Jm, 75.10.Dg, 75.30.Et

I. INTRODUCTION

Spin ice has proven to be one of the more fruitful marriages of theoretical and experimental condensed matter physics [1–5]. This cooperative paramagnetic phase [6] is a magnetic analogue of common water ice [1,2], with proton displacements mapped to magnetic moments pointing in or out of the corner-shared tetrahedra of the pyrochlore lattice [7]. Spin ice displays an exponential number of low-energy states, and thus an associated extensive residual entropy [8,9]. This manifold is characterized by the ice rules specifying that on each tetrahedron, two spins must point in and two must point out. Generically referred to as a "Coulomb phase" [10,11], the spin ice state harbors a rich phenomenology such as bow-tie shaped singularities (pinch points) in the magnetic structure factor [11,12] and gapped low-energy excitations, the latter providing a condensed matter realization of "magnetic monopoles" [4,10].

The two textbook materials that realize this spin ice physics are the pyrochlore rare-earth titanates [3] $Ho_2Ti_2O_7$ [7] and $Dy_2Ti_2O_7$ [8]. Significant evidence has accumulated that their magnetic and thermodynamic properties [10,13–15] can be quantitatively described by a classical model that includes nearest-neighbor exchange and long-range magnetostatic dipole-dipole interactions, both of *purely* Ising type. Amendments incorporating Ising interactions beyond nearest neighbors have been proposed to account for various fine details in the thermodynamic and magnetic behavior of $Dy_2Ti_2O_7$ [14,16,17]. The combination of Ising exchanges and long-range dipolar interactions is expected to lift the degeneracy of the ice manifold and release the residual entropy at very low temperatures [18–21]. Experimentally, such a transition has yet to be observed [22], with further significant deviations [23,24] from predictions raising questions to the completeness of the classical dipolar Ising spin-ice model [16]. In particular, one could speculate that the observed rise of the magnetic specific heat below ∼500 mK [23] is an indication that quantum effects are becoming important [25,26].

This classical Ising description [13,15,27] of the interactions has framed the theoretical and experimental perspectives [1–5] on these materials going back to their initial discovery [7,8]. Beyond its empirical successes, this mind set [13–21,27] is rooted in the *single-ion* magnetic properties of Dy^{3+} [8,22,28–30] and Ho^{3+} [7,27,31–33], specifically in the Ising nature of the crystal electric field (CEF) ground doublet of these ions. A consequence of this strict Ising anisotropy is that the transverse components of the total angular momentum, $J^{\pm}$, *vanish* between states of the CEF doublet. This is sufficient to explain the Ising form of any bilinear, anisotropic exchange interactions $\sim J_i^{\mu} K_{ij}^{\mu\nu} J_j^{\nu}$, including the long-range dipolar interactions [2]. The theoretical basis of the classical Ising description of spin ices then appears to rest on the implicit assumption that interactions between the rare-earth ions takes such a bilinear form. This common assumption is in fact *incorrect*; due to the large spin-orbit coupling in rare-earth ions, strong multipolar interactions between the J_i^{μ} momenta are generated when the microscopic superexchange is downfolded into the free-ion $^{2S+1}L_J$ manifold [34]. Indeed, this argument has been invoked [35] to show that quadrupolar interactions may not be negligible in Pr-based pyrochlore oxides with strictly Ising moments, such as $Pr_2Sn_2O_7$ [36] and $Pr_2Zr_2O_7$ [37]. Further compounding the problem is the possibility that even moderate transverse couplings could preempt the ordering expected from the dipolar interactions [18,21]. The existence of other spin ice compounds, such as $Ho_2Sn_2O_7$ [29,38], $Dy_2Sn_2O_7$ [29,39], $Ho_2Ge_2O_7$ [33,40], and $Dy_2Ge_2O_7$ [30,40] makes an explanation through some accidental fine-tuning unlikely. An unanswered puzzle thus lies in the identification of $Dy_2Ti_2O_7$ and $Ho_2Ti_2O_7$ as spin ices: why are these compounds so well described by a classical Ising model down to low temperatures? What principles, if any, constrain the scale of the multipolar interactions and suppress significant quantum fluctuations?

In this article, we explain why quantum effects in Dy- and Ho-based spin ice materials are very small, providing

approximate upper bounds on their size. First, in Sec. II, we review the effective pseudospin descriptions of $Dy_2Ti_2O_7$ and $Ho_2Ti_2O_7$, highlighting the structure of their CEF ground doublet and the symmetry-allowed transverse exchange interactions. Next, in Sec. III, we outline sources of exchange interactions and show that only magnetic dipole-dipole (MDD) and superexchange between the rare-earth ions are non-negligible at experimentally relevant temperatures. As the MDD interaction is purely Ising when projected into the ground CEF doublet, we therefore focus on superexchange. In Sec. IV, using a microscopic model of the oxygen charge transfer processes, we find that the resulting multipolar inter-ionic couplings arising from superexchange are strongly suppressed beyond rank seven. Because of the composition of the ground doublet, operators of rank seven or less can only connect its subleading spectral components and transverse (non-Ising) couplings in the low-energy theory are thus highly suppressed. From experimental constraints, in Sec. V we estimate them to be roughly two orders of magnitude smaller than the nearest-neighbor Ising coupling. More concretely, we carry out a model calculation in Sec. VI of the superexchange interaction in $Dy_2Ti_2O_7$ and $Ho_2Ti_2O_7$. This calculation corroborates our argument and provides explicit estimates for the size of quantum effects in the $Ho_2Ti_2O_7$ and $Dy_2Ti_2O_7$ spin ices. Finally, in Sec. VII, we discuss the implications of these arguments for finding quantum effects in other spin ices and more broadly in rare-earth pyrochlores in general.

II. PSEUDOSPIN MODELS

Our goal is to understand the interactions acting between the low-energy states of the CEF manifold in $Dy_2Ti_2O_7$ and $Ho_2Ti_2O_7$. We thus first review the structure of the low-energy pseudospin degrees of freedom for each of these compounds and their symmetry allowed transverse exchanges.

A. Dysprosium titanate

In $Dy_2Ti_2O_7$, the CEF ground doublet is a Kramers doublet built from states in the $^6H_{15/2}$ manifold of the $4f^9$ configuration of Dy^{3+}. For a realistic CEF potential [31,41], the ground state is a doublet with a gap of $\sim$30 meV to the first excited level. This doublet transforms in the $\Gamma_5 \oplus \Gamma_6$ representation of the site symmetry group D_{3d} and has Ising-like character, as shown below [42]. The doublet states are written as

$$|\pm\rangle = \alpha\left|\pm\tfrac{15}{2}\right\rangle \pm \delta_1\left|\pm\tfrac{9}{2}\right\rangle - \delta_2\left|\pm\tfrac{3}{2}\right\rangle \mp \delta_3\left|\mp\tfrac{3}{2}\right\rangle + \delta_4\left|\mp\tfrac{9}{2}\right\rangle \pm \delta_5\left|\mp\tfrac{15}{2}\right\rangle, \quad (1)$$

where $|M\rangle \equiv |15/2, M\rangle$ are eigenstates of the J^2 and J^z operators of the $^6H_{15/2}$ manifold. We choose the doublet basis so that $\delta_2\delta_3 - 3\delta_1\delta_4 + 5\alpha\delta_5 = 0$ to make the J^z dipole operator diagonal. The matrix elements of the magnetic dipole operators then are

$$\langle\sigma|J^{\pm}|\sigma'\rangle = 0, \quad \langle\sigma|J^z|\sigma'\rangle = \lambda\sigma\delta_{\sigma\sigma'}, \quad (2)$$

where $\sigma = \pm$ and the λ factor is

$$\lambda \equiv \tfrac{15}{2} - 3\left(\delta_1^2 + 2\delta_2^2 + 3\delta_3^2 + 4\delta_4^2 + 5\delta_5^2\right). \quad (3)$$

Including the Dy^{3+} Landé factor $g = 4/3$, the magnetic moment $\mu = g\mu_B\lambda$ is nearly maximal with estimates from the saturation magnetization and high-temperature susceptibility [22,28] giving $\mu = (10 \pm 0.1)\ \mu_B$. This constrains the $|\pm\rangle$ states in Eq. (1) to be predominantly $|\pm 15/2\rangle$ [8,31]. We thus have an upper bound of $\delta_n^2 \lesssim 0.025/n$ given the assumed $\pm 0.1\ \mu_B$ error bars.

Since the gap to first excited CEF doublet is large, it is sufficient to first consider only a bare projection of the microscopic Dy^{3+}-Dy^{3+} interactions into the ground doublet. Such a model can be expressed in terms of the components of a pseudospin 1/2 operator:

$$S^{\pm} = |\pm\rangle\langle\mp|, \quad S^z = \tfrac{1}{2}(|+\rangle\langle+| - |-\rangle\langle-|). \quad (4)$$

Symmetry restricts the nearest-neighbor effective exchange model for $Dy_2Ti_2O_7$ to the form [42]

$$\sum_{\langle ij\rangle}\left[J_{xx}S_i^xS_j^x + J_{yy}S_i^yS_j^y + J_{zz}S_i^zS_j^z + J_{xz}\left(S_i^zS_j^x + S_i^xS_j^z\right)\right]. \quad (5)$$

Since the $J_{\mu\nu}$ are *not* bond dependent, J_{xz} can be removed by a global rotation of the pseudospin operators about the local $\hat{y}$ axis [42], yielding

$$\sum_{\langle ij\rangle}\left[J_xS_i^xS_j^x + J_yS_i^yS_j^y + J_zS_i^zS_j^z\right]. \quad (6)$$

This model hosts a $U(1)$ quantum spin liquid [42] for $J_x, J_y \ll J_z$, and realizes a Z_2 spin liquid in a [111] magnetic field [43]. We find below that the net J_{zz}, including *both* the contribution from microscopic interionic superexchange *and* from the nearest-neighbor MDD interactions, is dominant and positive, as found empirically in Ref. [13]. At leading order in J_{xz}/J_{zz}, the rotated couplings are

$$J_x \sim J_{xx} - \frac{J_{xz}^2}{J_{zz}}, \quad J_y = J_{yy}, \quad J_z \sim J_{zz} + \frac{J_{xz}^2}{J_{zz}}. \quad (7)$$

This rotation affects the relationship between the components of the dipole moment and those of the pseudospin 1/2 at $O(J_{xz}/J_{zz})$. In $Dy_2Ti_2O_7$, we characterize deviations from the Ising limit in using the nearest-neighbor transverse scale $J_\pm \equiv (J_x + J_y)/4$ [42].

B. Holmium titanate

In the case of $Ho_2Ti_2O_7$, the crystal field (CEF) ground state is a non-Kramers doublet built from the $^5I_8$ manifold of the $4f^{10}$ configuration [7,31]. The first excited CEF level is $\sim$20 meV above the ground doublet [31]. This non-Kramers doublet transforms in the E_g representation of the D_{3d} site symmetry group and can be written

$$|\pm\rangle = \alpha|\pm 8\rangle \mp \delta_1|\pm 5\rangle + \delta_2|\pm 2\rangle \mp \delta_3|\mp 1\rangle + \delta_4|\mp 4\rangle \mp \delta_5|\mp 7\rangle, \quad (8)$$

where $|M\rangle \equiv |8, M\rangle$ are eigenstates of the J^2 and J^z operators of the $^5I_8$ manifold. This doublet is naturally Ising-like with

$$\langle\sigma|J^{\pm}|\sigma'\rangle = 0, \quad \langle\sigma|J^z|\sigma'\rangle = \lambda\sigma\delta_{\sigma\sigma'}, \quad (9)$$

where $\sigma = \pm$ and the λ factor is

$$\lambda \equiv 8 - 3\left(\delta_1^2 + 2\delta_2^2 + 3\delta_3^2 + 4\delta_4^2 + 5\delta_5^2\right). \quad (10)$$

Including the Ho^{3+} Landé factor, $g = 5/4$, the magnetic moment $\mu = g\mu_B\lambda$ is found to be very close to the maximal 10 μ_B experimentally [7,32,44]. This constrains the spectral content of the $|\pm\rangle$ states in Eq. (8) to be predominantly $|\pm 8\rangle$. We can also appeal to more detailed information on the CEF structure. Fits to the CEF levels obtained via neutron scattering have yielded estimates of the subleading components δ_n. For example, Ref. [41] gives

$$\begin{aligned} &\delta_1 = 0.189, \quad \delta_2 = 0.014, \quad \delta_3 = 0.070, \\ &\delta_4 = 0.031, \quad \delta_5 = 0.005. \end{aligned} \tag{11}$$

Rather than rely on these parameters, we shall consider the bound implied by a deviation of the moment from maximal by some amount ϵ, explicitly as $\mu = 10\mu_B \times (1-\epsilon)$. In $Dy_2Ti_2O_7$, we used $\epsilon = 0.01$ due to the $\pm 0.1\mu_B$ error bar from Ref. [22]. For $Ho_2Ti_2O_7$, this relation is $\delta_n^2 \lesssim 8\epsilon/(3n)$, but given the lack of stated bound on the moment, we use a more conservative $\epsilon = 0.05$, which implies $\delta_n^2 \lesssim 0.133/n$.

We proceed similarly to the $Dy_2Ti_2O_7$ case. Since the CEF energy scale is large [31], it is sufficient to first consider only a bare projection of the microscopic Ho^{3+}-Ho^{3+} interactions acting within the full $^5I_8$ manifold into the ground doublets. Again, such a model can be expressed in terms of the pseudospin 1/2 operators acting within the low-energy Hilbert space spanned by the $|\pm\rangle$ doublets, exactly as in Eq. (4). The symmetry of the pyrochlore lattice constrains the form of any such projected Hamiltonian. For a non-Kramers doublet, a nearest-neighbor model is restricted to the form [35,45,46]

$$\begin{aligned} \sum_{\langle ij\rangle} \big[& J_{zz} S_i^z S_j^z - J_\pm (S_i^+ S_j^- + S_i^- S_j^+) \\ & + J_{\pm\pm} (\gamma_{ij} S_i^+ S_j^+ + \gamma_{ij}^* S_i^- S_j^-) \big], \end{aligned} \tag{12}$$

where the bond-dependent phases γ_{ij} are defined in Ref. [45]. Once dipolar interactions are included, we will find below that J_{zz} is the dominant bare coupling and that it is positive, as is found experimentally [15]. In $Ho_2Ti_2O_7$, we characterize deviations from the Ising limit using the nearest-neighbor transverse scale $J_\pm$, as quantum effects from $J_{\pm\pm}$ appear at higher order in perturbation theory in $J_\perp/J_{zz}$ [45,46].

III. INTERACTIONS IN RARE-EARTH PYROCHLORES

Understanding how the microscopic interionic coupling mechanisms generate $J_\pm$ necessitates a description beyond the lowest CEF doublet. At the atomic level, there is a hierarchy of energy scales for the rare-earth ions: the Coulomb interaction being largest, followed by spin-orbit coupling and the CEF potential. The Coulomb interaction plays two roles: it provides the repulsion that separates the different $4f^n$ charge states and splits each $4f^n$ manifold into approximate fixed orbital and spin angular momenta ^{2S+1}L [47]. Spin-orbit coupling lifts the degeneracy of the states with the same total angular momentum J, giving the terms $^{2S+1}L_J$. Finally, the spherical symmetry of the ion is broken by the CEF and the $^{2S+1}L_J$ manifolds are further split into CEF multiplets.

To take into account this higher energy physics, we must move one level up from the ground doublet, and consider interactions within the $^6H_{15/2}$ or $^5I_8$ manifold of $Dy_2Ti_2O_7$ or $Ho_2Ti_2O_7$. Because of the spherical symmetry of the free ions, it is useful to categorize operators in terms of their *rank* as spherical tensors. Due to the large value J = 15/2 in the $^6H_{15/2}$ manifold of $Dy_2Ti_2O_7$, multipolar interactions up to rank 15 are possible [34]. In $Ho_2Ti_2O_7$ this is even larger, with J = 8 in the $^5I_8$ manifold allowing interactions up to rank-16. Interactions at this level will typically be on the order of ∼1 K, as inferred from the Curie-Weiss temperature [7,8]. Since the CEF energy scale is of order 300 K [31] in both $Dy_2Ti_2O_7$ and $Ho_2Ti_2O_7$, it is sufficient to consider only the projection into the ground doublet. Perturbative corrections are then expected at second order [48] with scale of $\sim(1\text{ K})^2/300\text{ K} \sim 3$–$5$ mK and thus can be neglected. There are several sources of interactions between rare-earth ions: electro- and magnetostatic interactions, superexchange, direct exchange, lattice-mediated exchange, etc. Of these, the MDD and superexchange interactions are found to be the most significant, as discussed in Appendix D.

The long-range MDD interaction features prominently in classical spin ices [13–15,27]. When projected into the ground doublet, it takes the form

$$\mathscr{D} \sum_{i<j} S_i^z S_j^z \left(\frac{r_{nn}}{r_{ij}}\right)^3 [\hat{z}_i \cdot \hat{z}_j - (\hat{r}_{ij} \cdot \hat{z}_i)(\hat{r}_{ij} \cdot \hat{z}_j)], \tag{13}$$

where r_{nn} is the nearest-neighbor distance between the rare-earth atoms, $\vec{r}_{ij} \equiv \vec{r}_i - \vec{r}_j$ is the displacement vector between the two sites and $\hat{z}_i$ is the quantization axis along the local cubic [111] direction at site $\vec{r}_i$. The strength of the coupling is characterized by $\mathscr{D} = g^2\lambda^2\mu_B^2\mu_0/(4\pi r_{nn}^3)$. The largest piece is the nearest-neighbor contribution, with coefficient $D \equiv 5\mathscr{D}/3$, which is ∼8.9 K [16] in $Dy_2Ti_2O_7$ and ∼9.4 K [15] in $Ho_2Ti_2O_7$ [49]. To obtain a quantitative agreement with experiments, corrections to the Ising couplings must be included. The nearest-neighbor correction J is the largest, estimated to be ∼4.55 K in $Dy_2Ti_2O_7$ [13,16] and ∼2.08 K in $Ho_2Ti_2O_7$ [19]. This coupling has usually been attributed to superexchange between the rare-earth ions and provides an indication of its overall scale [50]. We are thus confronted with the question: with such a large scale, why does superexchange not generate significant transverse couplings $J_\pm$?

IV. OXYGEN-MEDIATED SUPEREXCHANGE

To answer this question, we consider superexchange interactions mediated by the oxygen atoms that surround each rare-earth ion, singling out one exchange path consisting of two rare earths and one oxygen for simplicity. For the rare-earth sites, we define the creation operators $f_{1\alpha}^\dagger$ and $f_{2\alpha}^\dagger$ while for the intermediate oxygen site we use $p_\alpha^\dagger$. A combined index $\alpha \equiv (m,\sigma)$, where m and σ label the orbital and spin, is used throughout. Due to the localized nature of the rare-earth ions, we start with the atomic Hamiltonian at each site:

$$H_0 \equiv H_{f,1} + H_{f,2} + H_p, \tag{14}$$

where $H_{f,1}$ and $H_{f,2}$ are the atomic Hamiltonian for the two rare-earth ions and H_p for the oxygen site. On the oxygen site, we consider only the atomic potential Δ_{pf} and the cost to place two holes together on the same oxygen, U_p. We will not invoke the details of the rare-earth atomic Hamiltonian, aside from selecting the $^6H_{15/2}$ manifold of the $4f^9$ configuration.

We perturb H_0 with the hybridization terms,

$$V \equiv \sum_{\alpha\beta}[t_{1,\alpha\beta} f_{1\alpha}^\dagger p_\beta + t_{2,\alpha\beta} f_{2\alpha}^\dagger p_\beta + \text{H.c.}], \tag{15}$$

which represent electron hopping between the orbitals of the rare-earth and oxygen ions. Superexchange interactions are generated at fourth-order in perturbation theory [35] in V. For the details of the charge-transfer processes, see Appendix A.

To simplify the resolvent operators that appear in the perturbative expansion [51], we follow Ref. [35] and make the common "charging approximation," which states that only the charging energies $E(f^{n\pm1}) - E(f^n) \equiv U_f^\pm$ are significant. This neglects all other intra-atomic splittings in the energy denominators, such as those due to Hund's coupling or spin-orbit coupling. The energies $U_f^\pm$ are expected to be of order 5–10 eV in $4f$ compounds [52]. Within this approximation, the effective Hamiltonian is [35]

$$H_{\text{eff}} = \sum_{\alpha\beta\mu\nu}(P_1 f_{1\alpha}^\dagger f_{1\beta} P_1)\mathcal{I}_{12}^{\alpha\beta\mu\nu}(P_2 f_{2\mu}^\dagger f_{2\nu} P_2), \tag{16}$$

where P_i projects into the ground-state manifold of $H_{f,i}$ at site i. The interaction matrix $\mathcal{I}$ is defined as

$$\begin{aligned}\mathcal{I}_{12}^{\alpha\beta\mu\nu} \equiv \frac{2}{(U_f^+ + \Delta_{pf})^2}\Bigg[&- \frac{2[t_2 t_2^\dagger]^{\mu\nu}[t_1 t_1^\dagger]^{\alpha\beta}}{2U_f^+ + U_p + 2\Delta_{pf}} \\ &+ \left(\frac{1}{U_f^+ + U_f^-} + \frac{2}{2U_f^+ + U_p + 2\Delta_{pf}}\right) \\ &\times [t_2 t_1^\dagger]^{\mu\beta}[t_1 t_2^\dagger]^{\alpha\nu}\Bigg].\end{aligned} \tag{17}$$

We have dropped single-site terms that only renormalize the on-site single-ion Hamiltonian.

Generically, the interactions $\mathcal{I}$ are complicated due to the f^n states that make up the $^6\text{H}_{15/2}$ and $^5\text{I}_8$ manifolds of Dy^{3+} and Ho^{3+}. However, a strong constraint arises from the one-electron form $f_\alpha^\dagger f_\beta$ taken by the operators at each rare-earth site. When projected into the $^6\text{H}_{15/2}$ or $^5\text{I}_8$ manifold, these operators can generate only a small subset of all possible interactions between the J = 15/2 degrees of freedom of Dy^{3+} or the J = 8 degrees of freedom of Ho^{3+}. This can be seen explicitly by considering how these operators transform under rotations. Since each f electron carries a total angular momentum J = 5/2 or J = 7/2, the operators $f_\alpha^\dagger f_\beta$ are multipoles with rank ranging from rank 0 (5/2 − 5/2 or 7/2 − 7/2) up to rank 7 (7/2 + 7/2). Hence *only multipolar interactions up to and including rank-7 multipoles are generated by superexchange*. Because of the spherical symmetry of the free ions, the complicated intra-atomic interactions are rank-0 operators and thus *do not* change the rank-counting above. For a detailed argument for this point, see Appendix B. Including the CEF splittings in the resolvents only changes the above result slightly. Given the small overall splitting $\Delta \lesssim 100$ meV induced by the CEF [31,41], we can treat this as a perturbation to H_0 along with V. Since the CEF potential is a one-electron operator and is time-reversal invariant, it contains only operators up to rank 6, following similar reasoning as above [53]. Each inclusion of the CEF operator can thus increase the rank by 6, with up to rank-13 operators at order $\sim\Delta/U_f^\pm$, and operators up to the maximal rank 15 for Dy^{3+} or rank-16 for Ho^{3+} at order $\sim(\Delta/U_f^\pm)^2$. The rank-15 or rank-16 operators that directly link the leading $|\pm 15/2\rangle$ components in Dy^{3+} or the $|\pm 8\rangle$ components in Ho^{3+} are thus *strongly suppressed* by a factor of $(\Delta/U_f^\pm)^2 \sim 10^{-4}$. We can thus ignore these small corrections and can consider only interactions of rank 7 or lower.

The statement that multipolar interactions up to rank 7 are generated by superexchange can be found, either implicitly or explicitly, in a number of early works on superexchange in rare-earths; see, for example, Refs. [54,55,34,35]. The very recent work of Ref. [56] also explicitly points this out. Our results extend these arguments for this bound found in the literature in three essential ways: (i) we offered a complete treatment of the oxygens, not just as an effective f-f hopping, (ii) we showed that this holds beyond the charging approximation, for arbitrary spherically symmetric atomic interactions, and (iii) we discussed how the bound *fails* when the crystal field is included in the atomic problem.

V. GENERAL ARGUMENT

Returning to a more general physical picture, the results of Secs. III and IV allow us to explain why quantum effects are small in the dipolar spin ices $Dy_2Ti_2O_7$ and $Ho_2Ti_2O_7$. Given the dominant $|\pm 15/2\rangle$ or $|\pm 8\rangle$ CEF ground states in Dy^{3+} and Ho^{3+} [31] discussed in Sec. III, a large transverse scale $J_\pm$ would have to originate from *very* high-rank multipole interactions. However, these multipole interactions are only generated weakly from superexchange contributions, as they are much higher than rank 7, as discussed in Sec. IV. Due to this suppression, the leading contributions to the transverse couplings must come from the subdominant spectral components of the CEF ground doublet, the δ_n components given in Eq. (1) for $Dy_2Ti_2O_7$ or in Eq. (8) for $Ho_2Ti_2O_7$. When these are included, generation of $J_\pm$ by superexchange becomes feasible. As a rough estimate, if J is the typical scale of contributions from superexchange, then we expect

$$J_\pm \sim \left(\frac{\delta}{\alpha}\right)^2 J, \quad J_z \sim -J, \tag{18}$$

where δ represents the maximum size of the subdominant components of the CEF doublet. Each transverse pseudospin operator $S^\pm$ contributes one factor of δ/α to the scale $J_\pm$ [57]. Since we can constrain $\delta/\alpha \lesssim 0.1$ via the size of the magnetic moment, then one expects, all things being equal, the transverse scale $J_\pm$ to be suppressed by two orders of magnitude relative to the superexchange contributions to the Ising coupling J_z. Since we know $J \sim 5$ K in $Dy_2Ti_2O_7$ [13,16] and $J \sim 2$ K in $Ho_2Ti_2O_7$ [15], this implies $J_\pm \lesssim 50$ mK. This is the main conclusion of our work.

VI. ESTIMATE FROM MODEL CALCULATION

The simple argument of Sec. V does not include combinatoric factors or other unforeseen quirks or cancellations that could favor or disfavor the generation of transverse $J_\pm$ couplings. To check that such anomalies do not occur, we carry out an explicit calculation to verify this estimate. We work

within the charging approximation of Eq. (17), considering only a single superexchange path.

The shortest path between the rare-earth ions and oxygen passes through the $O(1)$ site situated in the center of each tetrahedron [3]. Within the Slater-Koster approximation [58], the hopping matrices t_1, t_2 can be expressed as $t_i = R_i^\dagger t_0$ where R_i is a rotation of the f and p orbitals that takes a set of axes aligned to the i local axes into the global frame. The matrices t_0 define overlaps in the frame aligned along the bond axis and take the simple form $[t_0]_{mm'} = \delta_{mm'}(\delta_{|m|,1} t_{pf\pi} + \delta_{m,0} t_{pf\sigma})$. We note that the precise values [59] of $t_{pf\pi}$ and $t_{pf\sigma}$ will not be important to our discussion. Since t_0 is diagonal and R_i is unitary, the products that appear in Eq. (17) are

$$[t_i t_j^\dagger]^{\alpha\beta} = t_0^\alpha t_0^\beta [R_i^\dagger R_j]^{\alpha\beta}, \quad [t_i t_i^\dagger]^{\alpha\beta} = \left(t_0^\alpha\right)^2 \delta_{\alpha\beta}, \tag{19}$$

as in Ref. [35]. Consideration of further superexchange paths between the other oxygen atoms would change the form of t_i, but not the overall multipolar structure of the interactions.

To evaluate the superexchange interactions, we proceed as follows: we first construct the CEF ground doublet states of Eqs. (1) and (8) from the full f^9 manifold for $Dy_2Ti_2O_7$ and the full f^{10} manifold for $Ho_2Ti_2O_7$. Next, we project the one-electron operators $f_\alpha^\dagger f_\beta$ into this basis. Finally, we sum these one-electron operators with the interaction constants of Eq. (17) evaluated using the t_i given above for single bond of the lattice. The remaining bonds can be recovered using the lattice symmetry. This gives a model of the form shown in Eq. (5) for $Dy_2Ti_2O_7$ and one of form Eq. (12) for $Ho_2Ti_2O_7$.

A. Dysprosium titanate

For $Dy_2Ti_2O_7$, at leading order in the δ_n coefficients, one obtains [60]

$$J_{xx} = -4J\left(\frac{\delta_5}{\alpha}\right)^2 + O(\alpha\delta^3), \quad J_{xz} = +2J\left(\frac{\delta_5}{\alpha}\right) + O(\alpha\delta^2),$$
$$J_{zz} = -J + O(\alpha\delta^2), \quad J_{yy} = 0 + O(\alpha\delta^3). \tag{20}$$

To perform this expansion we treat all δ_n as equally small. Practically speaking, we replace $\delta_n \to \eta\delta_n$ and expand to leading order in η, then send $\eta \to 1$. Statements such as $O(\delta^2)$ imply the dropped terms involve a product of some pair of the δ_n. The superexchange energy scale J is

$$J = \frac{2\alpha^4 t_{pf\sigma}^4}{(U_f^+ + \Delta)^2}\left(\frac{1}{U_f^+ + U_f^-} + \frac{2}{2U_f^+ + U_p + 2\Delta}\right)$$
$$\times \frac{1}{2187}\left(121 + 96\left(\frac{t_{pf\pi}}{t_{pf\sigma}}\right)^2 + 450\left(\frac{t_{pf\pi}}{t_{pf\sigma}}\right)^4\right). \tag{21}$$

From Eqs. (20) and (21), we see that our naïve scaling argument of $J_\pm \sim (\delta/\alpha)^2 J$ does in fact hold in this more detailed calculation. We also note that the sign of the superexchange contribution to J_{zz} is negative, as was found empirically for $Dy_2Ti_2O_7$ [13,16]; frustration is provided by the nearest-neighbor part of the MDD, which is positive.

Only the superexchange contribution to J_{zz} has been computed here; when rotating to eliminate the J_{xz} coupling, we must also include the large contribution D to J_{zz} coming from the nearest-neighbor part of the MDD interactions. We thus shift $J_{zz} \to J_{zz} + D$ where D is given in Eq. (13). Using the approximate rotations of Eq. (7), we find $J_y \sim 0$ and

$$J_x = -\frac{4DJ}{D-J}\left(\frac{\delta_5}{\alpha}\right)^2, \quad J_z = D - J + \frac{4J^2}{D-J}\left(\frac{\delta_5}{\alpha}\right)^2. \tag{22}$$

From the constraint on the moment size, we find $\delta_5^2/\alpha^2 \leqslant 0.005$ so then $J_\pm \lesssim 56$ mK. At the temperature scale of interest, monopole excitations [10] are suppressed and quantum effects can proceed only through quantum tunneling *within* the spin ice manifold [61]. The strength of tunneling g appears perturbatively at third order in the transverse coupling [42,61,62] as $g \sim 12 J_\pm^3/J_z^2$. Using the above estimate, these quantum effects would only become relevant for temperatures $\lesssim$0.15 mK in $Dy_2Ti_2O_7$. In fact, this estimate could be reduced significantly depending on how close the subleading spectral components of $|\pm\rangle$ are to their maximal values allowed by the moment size. For example, using the CEF parameters of Ref. [41], one has $\delta_5 \sim 10^{-3}$, which is much smaller than the bound implied by $\delta_n^2 \lesssim 0.025/n$ from the moment, giving a significantly smaller transverse coupling $J_\pm$.

B. Holmium titanate

For $Ho_2Ti_2O_7$, at leading order in the δ_n coefficients, one obtains

$$J_\pm = +J \cdot \rho_\pm\left(\frac{t_{f\pi}}{t_{f\sigma}}\right)\left(\frac{\delta_5}{\alpha}\right)^2 + O(\alpha\delta^3), \tag{23a}$$

$$J_{\pm\pm} = -J \cdot \rho_{\pm\pm}\left(\frac{t_{f\pi}}{t_{f\sigma}}\right)\left(\frac{\delta_5}{\alpha}\right)^2 + O(\alpha\delta^3), \tag{23b}$$

$$J_{zz} = -J + O(\alpha^3\delta), \tag{23c}$$

where all of the δ_n have been considered at the same order in the expansion. The superexchange energy scale J is given by

$$J = \frac{4\alpha^4 t_{f\sigma}^4}{(U_f^+ + \Delta_{pf})^2}\left(\frac{1}{U_f^+ + U_f^-} + \frac{2}{2U_f^+ + U_p + 2\Delta_{pf}}\right) \tag{24}$$
$$\times \frac{1}{2187}\left(121 + 48\left(\frac{t_{f\pi}}{t_{f\sigma}}\right)^2 + 207\left(\frac{t_{f\pi}}{t_{f\sigma}}\right)^4\right). \tag{25}$$

The above $\rho_\pm$ and $\rho_{\pm\pm}$ are rational functions of the ratio $x \equiv t_{f\pi}/t_{f\sigma}$ and are defined as

$$\rho_\pm(x) = \frac{9x^2(160 - 8x + 7x^2)}{8(121 + 48x^2 + 207x^4)}, \tag{26}$$

$$\rho_{\pm\pm}(x) = \frac{9x^2(68 - 16x - 7x^2)}{16(121 + 48x^2 + 207x^4)}. \tag{27}$$

Reasonable values of the Slater-Koster ratio [59] satisfy $-1 < t_{f\pi}/t_{f\sigma} < 0$. For this range, we can bound these functions as

$$0 < \rho_\pm(t_{f\pi}/t_{f\sigma}) \lesssim 0.6, \quad 0 < \rho_{\pm\pm}(t_{f\pi}/t_{f\sigma}) \lesssim 0.15. \tag{28}$$

As in $Dy_2Ti_2O_7$, we see the scaling, $J_\pm \sim (\delta/\alpha)^2 J$ holds with no large combinatoric factors or spurious cancellations that could have spoiled the heuristic argument presented in Sec. V. We also note that the sign of the superexchange contribution to the J_{zz} is again, correctly negative [15]. Setting

the superexchange scale to $J = 2.08$ K from the experimental constraints [15], we then can estimate $J_\pm$ and $J_{\pm\pm}$ as

$$J_\pm \lesssim 1.25\ \text{K} \cdot \left(\frac{\delta_5}{\alpha}\right)^2, \quad |J_{\pm\pm}| \lesssim 0.31\ \text{K} \cdot \left(\frac{\delta_5}{\alpha}\right)^2. \quad (29)$$

For a moment size that deviates from maximal by $\epsilon = 0.05$, this δ_5/α ratio is bounded as $(\delta_5/\alpha)^2 \lesssim 0.027$, giving

$$J_\pm \lesssim 34\ \text{mK}, \quad |J_{\pm\pm}| \lesssim 8.5\ \text{mK}. \quad (30)$$

Here the relevant transverse scale is the $J_\pm$ that appears in the nearest-neighbor model (12). With $J_{zz} = D - J \sim 7.32$ K, the implied tunneling scale g is $\ll 0.1$ mK and thus is not experimentally relevant. We note that these estimates for $J_\pm$ and $J_{\pm\pm}$ scale linearly in the deviation from the maximal moment. For the CEF parameters of Ref. [41], we have $(\delta_5/\alpha)^2 \sim 10^{-6}$, and one would have to look at next order in the δ_n to get at the true leading behavior. It is unclear if the currently available fits of the CEF energy levels are sufficiently precise to provide a useful estimate of the true size of δ_5. Nonetheless, such considerations can only serve to lower the scale of $J_\perp$ from the bounds in Eq. (30).

VII. OUTLOOK

We have presented a general argument as to why transverse exchanges in the "classical" spin ices $Dy_2Ti_2O_7$ and $Ho_2Ti_2O_7$ are small. In particular, we have shown that the generation of the required high rank multipolar couplings needed to link the nearly maximal $|\pm J\rangle$ states of the CEF doublets are strongly suppressed. Using an approximate treatment of the oxygen mediated superexchange interaction, we have provided some heuristic bounds on the size of these couplings. The presence of all these factors can provide an explanation of classical spin ice behavior in the related germanates $Ho_2Ge_2O_7$ [33,40] and $Dy_2Ge_2O_7$ [30,40] or the stannates $Ho_2Sn_2O_7$ [29,38] and $Dy_2Sn_2O_7$ [29,39]. Further, these considerations may have some relevance in ultimately understanding the dynamics of these systems [63–66] as their mere existence depends crucially on the presence of transverse spin couplings. These criteria also suggest what features to look for to move away from the classical spin ice limit [5]. For example, compounds with Kramers ions and large Ising-like moments, but significant subleading components in their ground state CEF doublet could present quantum behavior at more experimentally relevant temperature scales [5]. If the subdominant terms become *too* large, this picture breaks down and we expect all symmetry allowed effective spin-1/2 exchanges to be of comparable magnitude. This is known to be the case for $Er_2Ti_2O_7$ [67] and $Yb_2Ti_2O_7$ [45], while similar considerations are expected to apply to $Tb_2Ti_2O_7$ or the family $Pr_2M_2O_7$ [35]. In this context, the spinel $CdEr_2Se_4$ [68] with Ising Er^{3+} moment is an intriguing example where this logic may apply.

Note added. After completion of this work, Refs. [56,69] appeared, reaching some similar conclusions on the interactions between $^{2S+1}L_J$ multiplets in rare-earth ions.

ACKNOWLEDGMENTS

We thank Zhihao Hao for useful discussions. This work was supported by the Natural Sciences and Engineering Research Council of Canada, the Canada Research Chair program (M.J.P.G., Tier 1), the Canadian Foundation for Advanced Research and the Perimeter Institute (PI) for Theoretical Physics. Research at PI is supported by the Government of Canada through Industry Canada and by the Province of Ontario through the Ministry of Economic Development & Innovation. M.G. acknowledges the hospitality and generous support of the Quantum Matter Institute at the University of British Columbia and TRIUMF where part of this work was completed.

APPENDIX A: GENERAL DISCUSSION OF SUPEREXCHANGE

Here we present a derivation of the form of the superexchange shown in Sec. IV as well as some explicit details on the rank-7 bound. As discussed there, we consider the bare Hamiltonian of the two rare-earth sites and the intermediate oxygen atom:

$$H_0 \equiv H_{f,1} + H_{f,2} + H_p. \quad (A1)$$

We perturb this with the hybridization terms

$$V \equiv \sum_{\alpha\beta} [t^\dagger_{1,\alpha\beta} p^\dagger_\alpha f_{1\beta} + t_{1,\alpha\beta} f^\dagger_{1\alpha} p_\beta + t^\dagger_{2,\alpha\beta} p^\dagger_\alpha f_{2\beta} + t_{2,\alpha\beta} f^\dagger_{2\alpha} p_\beta], \quad (A2)$$

Exchange interactions between the rare-earth ions come in at fourth-order in V. We follow Ref. [51] and write the effective Hamiltonian using the ground-state projector P and resolvent operator R as

$$P = \sum_{\alpha\in 0} |\alpha\rangle\langle\alpha|, \quad R = \sum_{a\neq 0} \frac{|a\rangle\langle a|}{E_0 - E_a}, \quad (A3)$$

where $|\alpha\rangle$ are the ground states of H_0 with energy E_0 and $|a\rangle$ are the excited states of H_0 with energies E_a. The fourth-order effective Hamiltonian is then [51]

$$\begin{aligned} H_{\text{eff}} = {} & PVRVRVRVP - PVR^2VPVRVP \\ & - PVR^2VRVPVP - PVRVR^2VPVP \\ & + PVR^2VPVPVP. \end{aligned} \quad (A4)$$

Now since $PVP = 0$, we can drop all but the first two terms $PVRVRVRVP$ and $PVR^2VPVRVP$. The latter can be factored as $(PVR^2VP)(PVRVP)$ and thus serves to cancel nonextensive contributions that arise from the first term.

We thus can simply use $H_{\text{eff}} \sim PVRVRVRVP$, taking care to consider only the associated set of (extensive) perturbative processes. At the lowest order, we need only to consider the excited configurations that can be built by moving at most two electrons between the rare-earth and oxygen sites. These types of intermediate states can be understood by considering the possible values for the oxygen electron number. The range of accessible states are illustrated in Figs. 1–3. Starting from the ground-state $f^n p^6 f^n$ configuration, one follows the colored arrows to trace out a given exchange path. Spin and orbital indices on the f and p electron operators have been suppressed for clarity. We see that only two distinct types of processes are needed at fourth order, process 1 (Fig. 1), which creates at most one hole on the oxygen and processes 2 and 3 (Figs. 2

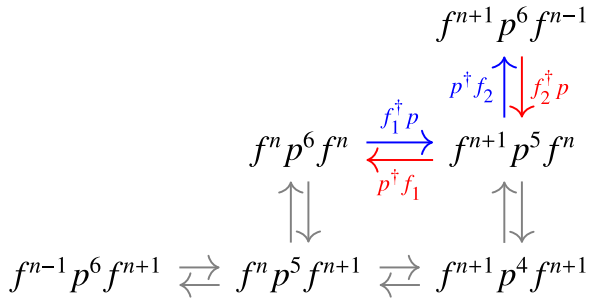

FIG. 1. (Color online) Process 1 involves intermediate states with only a single hole on the oxygen site. Scales roughly as $\sim t^4(U_f+\Delta_{pf})^{-2}(2U_f)^{-1}$.

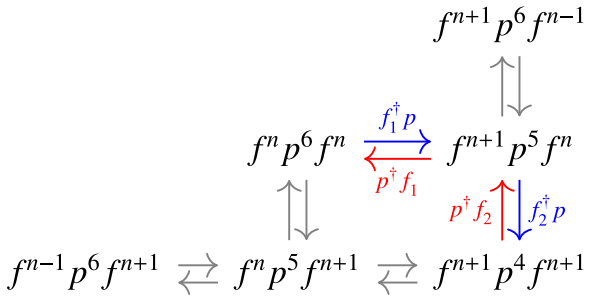

FIG. 3. (Color online) Process 3 involves an intermediate state with two holes on the oxygen site. Scales roughly as $\sim t^4(U_f+\Delta_{pf})^{-2}(2U_f+2\Delta_{pf}+U_p)^{-1}$.

and 3), which create an intermediate state with two holes on the oxygen. A second set of equivalent paths can be obtained by permuting the sites 1 and 2 in each process. Process 1 corresponds to the pieces of $H_{\rm eff}$ of the form

$$P[p^\dagger t_1^\dagger f_1]R[f_2^\dagger t_2 p]R[p^\dagger t_2^\dagger f_2]R[f_1^\dagger t_1 p]P. \tag{A5}$$

Each appearance of the resolvent operator R can be simplified given the restrictions created by the hybridization operator V. For example, the piece $[f_1^\dagger t_1 p]P$ can only involve states of the form $f^{n+1}p^5f^n$ since the ground-state manifold contains only states of the form $f^np^6f^n$. When acting on these states, the resolvent is simplified to an operator that acts only on the states of the rare-earth at site 1:

$$R_{f,1}\equiv\sum_{a\in f^{n+1}}\frac{|a\rangle_1\langle a|_1}{E_{f,a}-E_{f,0}+\Delta_{pf}}, \tag{A6}$$

where $|a\rangle$ are states of the f^{n+1} configuration and $E_{f,a}-E_{f,0}$ are their energies relative to the f^n ground state, and Δ_{pf} is the atomic potential of the oxygen site. An operator $R_{f,2}$ of identical form, can be defined acting only on site 2. The innermost resolvent can be simplified in the same way. Here, both rare-earth sites are involved, but the oxygen state is not. It can be replaced by the operator

$$R_{ff}^{(1)}\equiv\sum_{a\in f^{n+1}}\sum_{a'\in f^{n-1}}\frac{|a\rangle_1\langle a|_1|a'\rangle_2\langle a'|_2}{E_{f,a}+E_{f,a'}-2E_{f,0}}. \tag{A7}$$

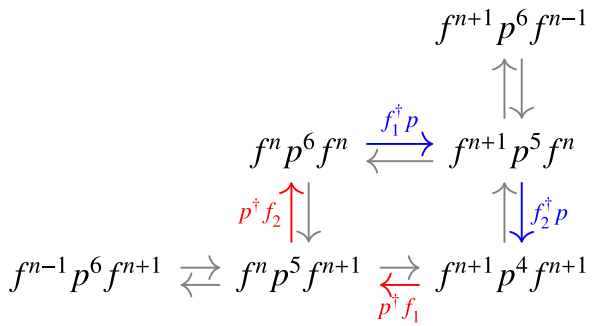

FIG. 2. (Color online) Process 2 involves an intermediate state with two holes on the oxygen site. Scales roughly as $\sim t^4(U_f+\Delta_{pf})^{-2}(2U_f+2\Delta_{pf}+U_p)^{-1}$.

This allows us to write the process 1 contribution as

$$P[p^\dagger t_1^\dagger f_1]R_{f,1}[f_2^\dagger t_2 p]R_{ff}^{(1)}[p^\dagger t_2^\dagger f_2]R_{f,1}[f_1^\dagger t_1 p]P. \tag{A8}$$

Now, since the resolvents no longer depend on the oxygen degrees of freedom, we can regroup this into oxygen and rare-earth parts:

$$\sum_{\alpha\beta\mu\nu}\sum_{\alpha'\beta'\mu'\nu'}[P_p p_\alpha^\dagger p_\beta p_\mu^\dagger p_\nu P_p][t_{1,\alpha\alpha'}^\dagger t_{2,\beta'\beta}t_{2,\mu\mu'}^\dagger t_{1,\nu'\nu}]$$
$$\times[P_f f_{1\alpha'}R_{f,1}f_{2\beta'}^\dagger R_{ff}^{(1)}f_{2\mu'}R_{f,1}f_{1\nu'}^\dagger P_f], \tag{A9}$$

where we have broken up the projector P into rare-earth (P_f) and oxygen parts (P_p) as $P\equiv P_fP_p$. The oxygen part is trivial with $P_pp_\alpha^\dagger p_\beta p_\mu^\dagger p_\nu P_p=\delta_{\mu\nu}\delta_{\alpha\beta}$. The final contribution from process 1 is then given by

$$P_f\left(\sum_{\alpha\beta\mu\nu}f_{1\alpha}R_{f,1}f_{2\beta}^\dagger R_{ff}^{(1)}f_{2\mu}R_{f,1}f_{1\nu}^\dagger[t_2t_1^\dagger]^{\beta\alpha}[t_1t_2^\dagger]^{\nu\mu}\right)P_f. \tag{A10}$$

We carry out the same argument for process 2. Following the arrows in Fig. 2, we find the contribution is

$$P[p^\dagger t_2^\dagger f_2]R[p^\dagger t_1^\dagger f_1]R[f_2^\dagger t_2 p]R[f_1^\dagger t_1 p]P. \tag{A11}$$

The outermost resolvents can be simplified using $R_{f,1}$ and $R_{f,2}$ as defined above. The innermost resolvent needs a new definition,

$$R_{ff}^{(2)}\equiv\sum_{a\in f^{n+1}}\sum_{a'\in f^{n+1}}\frac{|a\rangle_1\langle a|_1|a'\rangle_2\langle a'|_2}{E_{f,a}+E_{f,a'}-2E_{f,0}+2\Delta_{pf}+U_p}, \tag{A12}$$

to take into account the additional oxygen holes and Coulomb repulsion in the $f^{n+1}p^4f^{n+1}$ states, as discussed in Sec. IV of the main text. This then gives the operator

$$P[p^\dagger t_2^\dagger f_2]R_{f,2}[p^\dagger t_1^\dagger f_1]R_{ff}^{(2)}[f_2^\dagger t_2 p]R_{f,1}[f_1^\dagger t_1 p]P. \tag{A13}$$

Once again we can factor out the oxygen part, writing the total contribution as

$$\sum_{\alpha\beta\mu\nu}\sum_{\alpha'\beta'\mu'\nu'}[P_p p_\alpha^\dagger p_\beta^\dagger p_\mu p_\nu P_p][t_{2,\alpha\alpha'}^\dagger t_{1,\beta\beta'}^\dagger t_{2,\mu'\mu}t_{1,\nu'\nu}]$$
$$\times\left[P_f f_{2\alpha'}R_{f,1}f_{1\beta'}R_{ff}^{(2)}f_{2\mu'}^\dagger R_{f,1}f_{1\nu'}^\dagger P_f\right]. \tag{A14}$$

The oxygen part is slightly less trivial this time with $P_p p^\dagger_\alpha p^\dagger_\beta p_\mu p_\nu P_p = \delta_{\beta\mu}\delta_{\alpha\nu} - \delta_{\alpha\mu}\delta_{\beta\nu}$ We thus have

$$P_f\Bigg[\sum_{\alpha\beta\mu\nu}\left(f_{2\alpha}R_{f,2}f_{1\beta}R^{(2)}_{ff}f^\dagger_{2\mu}R_{f,1}f^\dagger_{1\nu}\right) \times([t_2t_1^\dagger]^{\mu\beta}[t_1t_2^\dagger]^{\nu\alpha} - [t_2t_2^\dagger]^{\mu\alpha}[t_1t_1^\dagger]^{\nu\beta})\Bigg]P_f. \quad \text{(A15)}$$

Finally, for process 3, we can reuse all of the building blocks that we have put together so far. From Fig. 3, we directly write the contribution

$$P[p^\dagger t_1^\dagger f_1]R_{f,1}[p^\dagger t_2^\dagger f_2]R^{(2)}_{ff}[f_2^\dagger t_2 p]R_{f,1}[f_1^\dagger t_1 p]P. \quad \text{(A16)}$$

Following an identical argument to the previous section, we arrive at

$$P_f\Bigg[\sum_{\alpha\beta\mu\nu}\left(f_{1\alpha}R_{f,1}f_{2\beta}R^{(2)}_{ff}f^\dagger_{2\mu}R_{f,1}f^\dagger_{1\nu}\right) \times([t_2t_2^\dagger]^{\mu\beta}[t_1t_1^\dagger]^{\nu\alpha} - [t_2t_1^\dagger]^{\mu\alpha}[t_1t_2^\dagger]^{\nu\beta})\Bigg]P_f, \quad \text{(A17)}$$

by simply swapping the site 1 and site 2 labels in the latter part of the exchange path.

APPENDIX B: MULTIPOLE RANKS AND RESOLVENT OPERATORS

From the expressions above, we see that the interactions between the rare-earth ions can be represented by operators of the form $\sim f^\dagger_{i,\alpha}f_{i,\beta}$ mediated by the oxygens, intermingled with resolvents such as $R_{f,1}$, $R_{f,2}$, $R^{(1)}_{ff}$, and $R^{(2)}_{ff}$. As discussed in Sec. IV of the main text, we consider the case where the resolvents do not contain the CEF potential and are thus afforded the full spherical symmetry of the free ion. Because of this symmetry, we can write the resolvents in terms of spherically symmetric projectors into each set of degenerate levels. Expanding out these sums and rearranging terms, we find that contributions to each process take the form

$$\sim(f^\dagger_{1\alpha}O_1f_{1\beta})(f^\dagger_{2\mu}O_2f_{2\nu}), \quad \text{(B1)}$$

where O_1 and O_2 are operators acting on rare-earth sites 1 and 2 built from rank-0 spherically symmetric projectors. The same rank counting outlined in the main text within the charging approximation thus holds true; operators of the form $f^\dagger_{i,\alpha}O_if_{i,\beta}$ involve multipoles of rank 7 or lower.

APPENDIX C: CHARGING ENERGY APPROXIMATION

Here we give the details that link the general results to the final expressions for the charging approximation given in the main text. Recall that in this approximation one postulates the energies of the f^n states predominantly depend on the total electron number n. With this approximation, we write

$$R_{f,i} \sim \sum_{a\in f^{n+1}}\frac{|a\rangle_i\langle a|_i}{U_f^+ + \Delta_{pf}} \equiv \frac{1-P_f}{U_f^+ + \Delta_{pf}}, \quad \text{(C1)}$$

since $E_{f,a} - E_{f,0} \sim U_f^+$ for all states $|a\rangle \in f^{n+1}$. Since the structure of the perturbation forces us to be in the f^{n+1} state, we can extend the sum to all excited states and thus arrive at the projector $1 - P_f$. Applying the same approximation to the innermost resolvents, we find

$$R^{(1)}_{ff} \sim \frac{1-P_f}{U_f^+ + U_f^-}, \quad R^{(2)}_{ff} \sim \frac{1-P_f}{2U_f^+ + U_p + 2\Delta_{pf}}, \quad \text{(C2)}$$

where U_f^- is the energy difference $E_{f,a} - E_{f,0}$ when $|a\rangle$ is a state in the f^{n-1} manifold. We can now use these resolvents to simplify the contributions from the three processes (Figs. 1–3) considered earlier, and shown in Eqs. (A10), (A15), and (A17). In each expression, the ground-state projectors P_f drop out, and we can write the contributions from each of the three processes as

$$1: \frac{1}{(U_f^+ + \Delta_{pf})^2(U_f^+ + U_f^-)} \times P_f\left(\sum_{\alpha\beta\mu\nu} f_{1\alpha}f^\dagger_{2\beta}f_{2\mu}f^\dagger_{1\nu}[t_2t_1^\dagger]^{\beta\alpha}[t_1t_2^\dagger]^{\nu\mu}\right)P_f,$$

$$2: \frac{1}{(U_f^+ + \Delta_{pf})^2(2U_f^+ + U_p + 2\Delta_{pf})} \times P_f\Bigg(\sum_{\alpha\beta\mu\nu} f_{2\alpha}f_{1\beta}f^\dagger_{2\mu}f^\dagger_{1\nu}([t_2t_1^\dagger]^{\mu\beta}[t_1t_2^\dagger]^{\nu\alpha} - [t_2t_2^\dagger]^{\mu\alpha}[t_1t_1^\dagger]^{\nu\beta})\Bigg)P_f,$$

$$3: \frac{1}{(U_f^+ + \Delta_{pf})^2(2U_f^+ + U_p + 2\Delta_{pf})} \times P_f\Bigg(\sum_{\alpha\beta\mu\nu} f_{1\alpha}f_{2\beta}f^\dagger_{2\mu}f^\dagger_{1\nu}([t_2t_2^\dagger]^{\mu\beta}[t_1t_1^\dagger]^{\nu\alpha} - [t_2t_1^\dagger]^{\mu\alpha}[t_1t_2^\dagger]^{\nu\beta})\Bigg)P_f.$$

We can further massage the expressions for each process to put the f operators into a standard order. Finally, the swapping of 1 and 2 generates an identical contribution and thus a factor of two. Collecting the contributions from all three processes and dropping any single-site operators generated by commuting the pieces, we obtain the final result for H_{eff}:

$$H_{\text{eff}} = \sum_{\alpha\beta\mu\nu}(P_{f,1}f^\dagger_{1\alpha}f_{1\beta}P_{f,1})\mathcal{I}_{12}^{\alpha\beta\mu\nu}(P_{f,2}f^\dagger_{2\mu}f_{2\nu}P_{f,2}), \quad \text{(C3)}$$

where the interaction matrix is defined as

$$\mathcal{I}_{12}^{\alpha\beta\mu\nu} \equiv \frac{2}{(U_f^+ + \Delta_{pf})^2}\Bigg[\left(\frac{1}{U_f^+ + U_f^-} + \frac{2}{2U_f^+ + U_p + 2\Delta_{pf}}\right) \times[t_2t_1^\dagger]^{\mu\beta}[t_1t_2^\dagger]^{\alpha\nu} - \frac{2[t_2t_2^\dagger]^{\mu\nu}[t_1t_1^\dagger]^{\alpha\beta}}{2U_f^+ + U_p + 2\Delta_{pf}}\Bigg], \quad \text{(C4)}$$

as given in Sec. IV of the main text. An alternative route to the superexchange interactions would be to integrate out the oxygen degrees of freedom first. This downfolding gives

an effective f-f hopping of order $t_{\rm eff} \equiv t^2/\Delta_{pf}$. Within the approach discussed here, this corresponds to taking $\Delta_{pf} \gg U_f^{\pm}$, eliminating all but process 1 at leading order, which involves only states with a single hole on the oxygen sites. This then takes the form of a second-order result in the effective hopping $t_{\rm eff}$. Such an approximation simplifies much of the above analysis, but leaves the main conclusion unchanged.

APPENDIX D: OTHER MICROSCOPIC INTERACTIONS

In this appendix, we outline some other possible sources of ion-ion interactions that act within the J = 15/2 and J = 8 manifolds of Dy^{3+} and Ho^{3+}, respectively.

1. Magnetic multipole interactions

Being of magnetostatic origin, the scale of the magnetic multipole interactions (MMI) are simple to address. These are only directly relevant for $Dy_2Ti_2O_7$, as the transverse couplings in non-Kramers doublet relevant for $Ho_2Ti_2O_7$ are time-reversal even [35]. Generally, the scale of the interaction between a rank-K and rank-K' magnetic multipole is approximately given by [70]

$$\mathcal{M}_{KK'} \sim \chi_{K-1}\chi_{K'-1}\langle r^{K-1}\rangle\langle r^{K'-1}\rangle\left(\frac{\mu^{K+K'}\mu_0}{4\pi}\right)\frac{1}{R^{K+K'+1}}, \tag{D1}$$

where χ_K is the order K Stevens' parameter [53], $\langle r^K\rangle$ is an atomic radial integral [71], μ is the magnetic moment of the ion, and R is the distance between the ions. This expression is somewhat conservative as we have assumed that the multipole moments are maximal, including factors of J^{K} and $\mathrm{J}^{\mathrm{K}'}$ in the expression for $\mu^{K+K'}$ where J = 15/2. Projecting into the ground-state doublet, quenches these moments and further reduces the estimate. This is especially true for $Dy_2Ti_2O_7$ where the ground-state doublet is primarily composed of $|\pm 15/2\rangle$ states and thus has predominantly rank-15 moments that could contribute the transverse couplings. Using $\mu \sim 10\ \mu_{\rm B}$, we find these MMI to be small beyond the dipole-dipole term $\mathcal{M}_{11} \sim 1.4$ K. The more useful number is $D \equiv 4(5\mathcal{M}_{11}/3) \sim 8.9$ K, as discussed in Sec. III of the main text. For dipole-octupole coupling, one finds $\mathcal{M}_{13} \sim -16$ mK, while for octupole-octupole, one finds $\mathcal{M}_{33} \sim 0.17$ mK. Given the factor of $R^{-(K+K'+1)}$, higher-rank interactions are quickly suppressed. The nearest-neighbor dipole-octupole coupling is largest and necessarily projects into exchanges of the form $\sim S_i^z S_j^x + S_i^x S_j^z$. Finally, one must take into account that when the octupole moments are projected into the ground-state doublet, their contribution is further reduced. The suppression factors are $\sim\delta/\alpha$, which reduce the dipole-octupole terms by a factor of $\sim$0.1 and the octupole-octupole terms by $\sim$0.01. The induced transverse terms are thus $\lesssim (\delta/\alpha\cdot\mathcal{M}_{13})^2/J_{zz} \sim 0.5\times 10^{-3}$ mK for the dipole-octupole coupling (after the rotation discussed in Sec. II A) and $\lesssim (\delta/\alpha)^2\mathcal{M}_{33} \sim 2\times 10^{-3}$ mK for the octupole-octupole coupling. The quantum effects are then completely negligible, and thus the MMI can be safely ignored beyond dipole-dipole interactions as used in Sec. III.

2. Electric multipole interactions

Being time-reversal even, electric multipole interactions (EMI) are only directly relevant for $Ho_2Ti_2O_7$ as the transverse components in the Kramers ground doublet of $Dy_2Ti_2O_7$ are time-reversal odd. Generally, the scale of the EMI between a rank-K and rank-K' electric multipole is approximately given by [72]

$$\mathcal{E}_{KK'} \sim \chi_K\chi_{K'}\langle r^K\rangle\langle r^{K'}\rangle\frac{\mathrm{J}^{K+K'}}{R^{K+K'+1}}\left(\frac{e^2}{4\pi\epsilon_0}\right), \tag{D2}$$

where e is the elementary charge, ϵ_0 is the permittivity of vacuum and the remainder of the notation is the same as in the previous section. We have included factors of J^K and $\mathrm{J}^{K'}$ to account for possible matrix element effects as conservatively as possible. The largest of these couplings is the electric quadrupole-quadrupole coupling at order $\mathcal{E}_{22} \sim 63$ mK. Due to the composition of the ground doublet, transverse couplings originating from EMI will carry additional factors of $\sim(\delta/\alpha)^2$, as in the MMI. The scale of these contributions are then $\lesssim$1 mK. Shielding effects [72] will reduce this number further. The higher order interactions are even smaller and so the electric multipolar interactions are not a significant source of transverse couplings in $Ho_2Ti_2O_7$.

3. Lattice mediated interactions

Additional interactions could be mediated through spin-phonon coupling [34,73–75]. Due to time-reversal symmetry, these can only directly generate interactions between multipoles of even rank. For $Dy_2Ti_2O_7$, these vanish under projection into the ground state CEF doublet, and thus do not contribute directly to the transverse terms. For $Ho_2Ti_2O_7$, such even-rank interaction can contribute directly to the transverse terms. To evaluate the plausibility of such a scenario, we consider two models of spin-phonon interaction: a site-phonon and bond-phonon models. In the site-phonon model, we consider only the coupling of the on-site multipoles to the local lattice distortion. In the same way as the CEF, when represented as Stevens' operator equivalents, these can only include operators up to rank 6. When the site-phonon is integrated out, these operators are squared so interactions up to a maximum of rank 12 can be generated. In a bond-phonon type model, we imagine the lattice distortion modifying the exchanges already present in the system. Given the argument in Sec. III, we expect these to be predominantly rank 7 or lower and thus when the phonon is integrated out, the induced interactions are rank 14 or smaller. Since these are not the direct rank-16 interactions needed to connect $|\pm 8\rangle$ to $|\mp 8\rangle$, they are suppressed by the subleading doublet components by the same mechanisms discussed in the main text. Additionally, there will be a further suppression from the energy scale of the phonon that must be integrated out. We thus can safely ignore the spin-lattice couplings in our analysis.

4. Direct exchange

We have already accounted for some of the intersite Coulomb interaction in our treatment of the electric multipole interactions (EMI). Other contributions such as direct exchange between the rare-earth ions is likely to be of the same

order or smaller given their large separation. Generally, one could write pair-wise direct exchange contributions in the form

$$\sum_{ij}\sum_{\alpha\beta\mu\nu}\mathcal{U}_{ij}^{\alpha\beta\mu\nu}f_{i\alpha}^{\dagger}f_{i\beta}f_{j\mu}^{\dagger}f_{j\nu}. \tag{D3}$$

As we have seen, the one-electron form of the operators at each site restrict this to generate multipolar interactions of rank 7 or less. Thus we have the same suppression factor $(\delta/\alpha)^2$ as discussed in Sec. V. Given the scale of the EMI, we then expect these terms to be negligible. We note that direct exchange interactions between the rare-earth and oxygen sites could be present. However, due to the need to include additional electron transfers to generate interactions and the filled shell of the oxygen site, we would expect these terms to be small.

[1] S. T. Bramwell and M. J. P. Gingras, Spin ice state in frustrated magnetic pyrochlore materials, Science **294**, 1495 (2001).

[2] M. J. P. Gingras, Spin ice, in *Introduction to Frustrated Magnetism*, Springer Series in Solid-State Sciences, Vol. 164, edited by C. Lacroix, P. Mendels, and F. Mila (Springer, Berlin, 2011).

[3] J. S. Gardner, M. J. P. Gingras, and J. E. Greedan, Magnetic pyrochlore oxides, Rev. Mod. Phys. **82**, 53 (2010).

[4] C. Castelnovo, R. Moessner, and S. L. Sondhi, Spin ice, fractionalization, and topological order, Annu. Rev. Condens. Matter Phys. **3**, 35 (2012).

[5] M. J. P. Gingras and P. A. McClarty, Quantum spin ice: A search for gapless quantum spin liquids in pyrochlore magnets, Rep. Prog. Phys. **77**, 056501 (2014).

[6] J. Villain, Insulating spin glasses, Z. Phys. B **33**, 31 (1979).

[7] M. J. Harris, S. T. Bramwell, D. F. McMorrow, T. Zeiske, and K. W. Godfrey, Geometrical Frustration in the Ferromagnetic Pyrochlore $Ho_2Ti_2O_7$, Phys. Rev. Lett. **79**, 2554 (1997).

[8] A. P. Ramirez, A. Hayashi, R. J. Cava, R. Siddharthan, and B. S. Shastry, Zero-point entropy in spin ice, Nature (London) **399**, 333 (1999).

[9] A. L. Cornelius and J. S. Gardner, Short-range magnetic interactions in the spin-ice compound $Ho_2Ti_2O_7$, Phys. Rev. B **64**, 060406 (2001).

[10] C. Castelnovo, R. Moessner, and S. L. Sondhi, Magnetic monopoles in spin ice, Nature (London) **451**, 42 (2008).

[11] C. L. Henley, The "Coulomb Phase" in frustrated systems, Annu. Rev. Condens. Matter Phys. **1**, 179 (2010).

[12] S. V. Isakov, K. Gregor, R. Moessner, and S. L. Sondhi, Dipolar Spin Correlations in Classical Pyrochlore Magnets, Phys. Rev. Lett. **93**, 167204 (2004).

[13] B. C. den Hertog and M. J. P. Gingras, Dipolar Interactions and Origin of Spin Ice in Ising Pyrochlore Magnets, Phys. Rev. Lett. **84**, 3430 (2000).

[14] J. P. C. Ruff, R. G. Melko, and M. J. P. Gingras, Finite-Temperature Transitions in Dipolar Spin Ice in a Large Magnetic Field, Phys. Rev. Lett. **95**, 097202 (2005).

[15] S. T. Bramwell, M. J. Harris, B. C. den Hertog, M. J. P. Gingras, J. S. Gardner, D. F. McMorrow, A. R. Wildes, A. L. Cornelius, J. D. M. Champion, R. G. Melko *et al.*, Spin Correlations in $Ho_2Ti_2O_7$: A Dipolar Spin Ice System, Phys. Rev. Lett. **87**, 047205 (2001).

[16] T. Yavors'kii, T. Fennell, M. J. P. Gingras, and S. T. Bramwell, $Dy_2Ti_2O_7$ Spin Ice: A Test Case for Emergent Clusters in a Frustrated Magnet, Phys. Rev. Lett. **101**, 037204 (2008).

[17] Y. Tabata, H. Kadowaki, K. Matsuhira, Z. Hiroi, N. Aso, E. Ressouche, and B. Fåk, Kagome Ice State in the Dipolar Spin Ice $Dy_2Ti_2O_7$, Phys. Rev. Lett. **97**, 257205 (2006).

[18] M. J. P. Gingras and B. C. den Hertog, Origin of spin-ice behavior in Ising pyrochlore magnets with long-range dipole interactions: an insight from mean-field theory, Can. J. Phys. **79**, 1339 (2001).

[19] R. G. Melko, B. C. den Hertog, and M. J. P. Gingras, Long-Range Order at Low Temperatures in Dipolar Spin Ice, Phys. Rev. Lett. **87**, 067203 (2001).

[20] R. G. Melko and M. J. P. Gingras, Monte carlo studies of the dipolar spin ice model, J. Phys.: Condens. Matter **16**, R1277 (2004).

[21] S. V. Isakov, R. Moessner, and S. L. Sondhi, Why Spin Ice Obeys the Ice Rules, Phys. Rev. Lett. **95**, 217201 (2005).

[22] H. Fukazawa, R. G. Melko, R. Higashinaka, Y. Maeno, and M. J. P. Gingras, Magnetic anisotropy of the spin-ice compound $Dy_2Ti_2O_7$, Phys. Rev. B **65**, 054410 (2002).

[23] D. Pomaranski, L. R. Yaraskavitch, S. Meng, K. A. Ross, H. M. L. Noad, H. A. Dabkowska, B. D. Gaulin, and J. B. Kycia, Absence of Pauling's residual entropy in thermally equilibrated $Dy_2Ti_2O_7$, Nat. Phys. **9**, 353 (2013).

[24] S. Scharffe, O. Breunig, V. Cho, P. Laschitzky, M. Valldor, J. F. Welter, and T. Lorenz, Suppression of Pauling's residual entropy in dilute spin ice $(Dy_{1-x}Y_x)_2Ti_2O_7$, arXiv:1503.03856 [cond-mat.str-el].

[25] N. Shannon, Magnetic monopoles: Entropy lost, Nat. Phys. **9**, 326 (2013).

[26] P. A. McClarty, O. Sikora, R. Moessner, K. Penc, F. Pollmann, and N. Shannon, Chain-based order and quantum spin liquids in dipolar spin ice, Phys. Rev. B **92**, 094418 (2015).

[27] R. Siddharthan, B. S. Shastry, A. P. Ramirez, A. Hayashi, R. J. Cava, and S. Rosenkranz, Ising Pyrochlore Magnets: Low-Temperature Properties, "Ice Rules", and Beyond, Phys. Rev. Lett. **83**, 1854 (1999).

[28] D. J. Flood, Magnetization and magnetic entropy of $Dy_2Ti_2O_7$, J. Appl. Phys. **45**, 4041 (1974).

[29] K. Matsuhira, Y. Hinatsu, K. Tenya, H. Amitsuka, and T. Sakakibara, Low-temperature magnetic properties of pyrochlore stannates, J. Phys. Soc. Jpn. **71**, 1576 (2002).

[30] X. Ke, M. L. Dahlberg, E. Morosan, J. A. Fleitman, R. J. Cava, and P. Schiffer, Magnetothermodynamics of the Ising antiferromagnet $Dy_2Ge_2O_7$, Phys. Rev. B **78**, 104411 (2008).

[31] S. Rosenkranz, A. P. Ramirez, A. Hayashi, R. J. Cava, R. Siddharthan, and B. S. Shastry, Crystal-field interaction in the pyrochlore magnet $Ho_2Ti_2O_7$, J. Appl. Phys. **87**, 5914 (2000).

[32] O. A. Petrenko, M. R. Lees, and G. Balakrishnan, Magnetization process in the spin-ice compound $Ho_2Ti_2O_7$, Phys. Rev. B **68**, 012406 (2003).

[33] A. M. Hallas, J. A. M. Paddison, H. J. Silverstein, A. L. Goodwin, J. R. Stewart, A. R. Wildes, J. G. Cheng, J. S. Zhou, J. B. Goodenough, E. S. Choi, G. Ehlers, J. S. Gardner, C. R. Wiebe, and H. D. Zhou, Statics and dynamics of the highly correlated spin ice $Ho_2Ge_2O_7$, Phys. Rev. B **86**, 134431 (2012).

[34] P. Santini, S. Carretta, G. Amoretti, R. Caciuffo, N. Magnani, and G. H. Lander, Multipolar interactions in f-electron systems:

The paradigm of actinide dioxides, Rev. Mod. Phys. **81**, 807 (2009).

[35] S. Onoda and Y. Tanaka, Quantum fluctuations in the effective pseudospin-$\frac{1}{2}$ model for magnetic pyrochlore oxides, Phys. Rev. B **83**, 094411 (2011).

[36] H. D. Zhou, C. R. Wiebe, J. A. Janik, L. Balicas, Y. J. Yo, Y. Qiu, J. R. D. Copley, and J. S. Gardner, Dynamic Spin Ice: $Pr_2Sn_2O_7$, Phys. Rev. Lett. **101**, 227204 (2008).

[37] K. Kimura, S. Nakatsuji, J. J. Wen, C. Broholm, M. B. Stone, E. Nishibori, and H. Sawa, Quantum fluctuations in spin-ice-like $Pr_2Zr_2O_7$, Nat. Comm. **4**, 1934 (2013).

[38] H. Kadowaki, Y. Ishii, K. Matsuhira, and Y. Hinatsu, Neutron scattering study of dipolar spin ice $Ho_2Sn_2O_7$: Frustrated pyrochlore magnet, Phys. Rev. B **65**, 144421 (2002).

[39] K. Matsuhira, M. Wakeshima, Y. Hinatsu, C. Sekine, C. Paulsen, T. Sakakibara, and S. Takagi, Slow dynamics of Dy pyrochlore oxides $Dy_2Sn_2O_7$ and $Dy_2Ir_2O_7$, J. Phys.: Conf. Ser. **320**, 012050 (2011).

[40] H. D. Zhou, J. G. Cheng, A. M. Hallas, C. R. Wiebe, G. Li, L. Balicas, J. S. Zhou, J. B. Goodenough, J. S. Gardner, and E. S. Choi, Chemical Pressure Effects on Pyrochlore Spin Ice, Phys. Rev. Lett. **108**, 207206 (2012).

[41] A. Bertin, Y. Chapuis, P. Dalmas de Réotier, and A. Yaouanc, Crystal electric field in the $R_2Ti_2O_7$ pyrochlore compounds, J. Phys.: Condens. Matter **24**, 256003 (2012).

[42] Y. P. Huang, G. Chen, and M. Hermele, Quantum Spin Ices and Topological Phases from Dipolar-Octupolar Doublets on the Pyrochlore Lattice, Phys. Rev. Lett. **112**, 167203 (2014).

[43] J. Carrasquilla, Z. Hao, and R. G Melko, A two-dimensional spin liquid in quantum kagome ice, Nat. Commun. **6**, 7421 (2015).

[44] D. P. Leusink, F. Coneri, M. Hoek, S. Turner, H. Idrissi, G. Van Tendeloo, and H. Hilgenkamp, Thin films of the spin ice compound $Ho_2Ti_2O_7$, APL Mater. **2**, 032101 (2014).

[45] K. A. Ross, L. Savary, B. D. Gaulin, and L. Balents, Quantum Excitations in Quantum Spin Ice, Phys. Rev. X **1**, 021002 (2011).

[46] S. B. Lee, S. Onoda, and L. Balents, Generic quantum spin ice, Phys. Rev. B **86**, 104412 (2012).

[47] E. U. Condon and G. H. Shortley, *The Theory of Atomic Spectra* (Cambridge University Press, Cambridge, England, 1951).

[48] H. R. Molavian, M. J. P. Gingras, and B. Canals, Dynamically Induced Frustration as a Route to a Quantum Spin Ice State in $Tb_2Ti_2O_7$ via Virtual Crystal Field Excitations and Quantum Many-Body Effects, Phys. Rev. Lett. **98**, 157204 (2007).

[49] Note that some prior work use a different convention for their Ising variables, taking values ± 1 rather than the pseudospin $\pm 1/2$ used here. This accounts for a factor of four difference in the stated exchange constants D and J. Explicitly, the dipolar energy scale $D_{\rm nn}$ defined in Refs. [13,15] thus corresponds to $D/4$, and similarly for the nearest-neighbour correction.

[50] The sign convention for J is reversed relative to some prior work in Refs. [13,19,14,20].

[51] I. Lindgren, The Rayleigh-Schrödinger perturbation and the linked-diagram theorem for a multi-configurational model space, J. Phys. B **7**, 2441 (1974).

[52] D. van der Marel and G. A. Sawatzky, Electron-electron interaction and localization in d and f transition metals, Phys. Rev. B **37**, 10674 (1988).

[53] K. W. H. Stevens, Matrix elements and operator equivalents connected with the magnetic properties of rare earth ions, Proc. Phys. Soc. A **65**, 209 (1952).

[54] R. J. Elliott and M. F. Thorpe, Orbital effects on exchange interactions, J. Appl. Phys. **39**, 802 (1968).

[55] P. M Levy, Anisotropy in two-center exchange interactions, Phys. Rev. **177**, 509 (1969).

[56] N. Iwahara and L. F. Chibotaru, Exchange interaction between J-multiplets, Phys. Rev. B **91**, 174438 (2015).

[57] For the case of the $\Gamma_5 \oplus \Gamma_6$ doublet of $Dy_2Ti_2O_7$, the J_{xz} exchange will be of order δ/α, since only one of the pseudospins involved is transverse. Redefining the axes by the rotation of Eq. (7), we recover the estimate as stated.

[58] J. C. Slater and G. F. Koster, Simplified LCAO method for the periodic potential problem, Phys. Rev. **94**, 1498 (1954).

[59] K. Takegahara, Y. Aoki, and A. Yanase, Slater-Koster tables for f electrons, J. Phys. C **13**, 583 (1980).

[60] The leading dependence on only δ_5 may be a consequence of the high-symmetry of the superexchange path through the $O(1)$ ion.

[61] M. Hermele, M. P. A. Fisher, and L. Balents, Pyrochlore photons: The U(1) spin liquid in a S = 1/2 three-dimensional frustrated magnet, Phys. Rev. B **69**, 064404 (2004).

[62] Y. Kato and S. Onoda, Numerical Evidence of Quantum Melting of Spin Ice: Quantum-to-Classical Crossover, Phys. Rev. Lett. **115**, 077202 (2015).

[63] K. Matsuhira, Y. Hinatsu, and T. Sakakibara, Novel dynamical magnetic properties in the spin ice compound $Dy_2Ti_2O_7$, J. Phys.: Condens. Matter **13**, L737 (2001).

[64] J. Snyder, J. S. Slusky, R. J. Cava, and P. Schiffer, How 'spin ice' freezes, Nature (London) **413**, 48 (2001).

[65] J. A. Quilliam, L. R. Yaraskavitch, H. A. Dabkowska, B. D. Gaulin, and J. B. Kycia, Dynamics of the magnetic susceptibility deep in the coulomb phase of the dipolar spin ice material $Ho_2Ti_2O_7$, Phys. Rev. B **83**, 094424 (2011).

[66] H. M. Revell, L. R. Yaraskavitch, J. D. Mason, K. A. Ross, H. M. L. Noad, H. A. Dabkowska, B. D. Gaulin, Patrik Henelius, and J. B. Kycia, Evidence of impurity and boundary effects on magnetic monopole dynamics in spin ice, Nat. Phys. **9**, 34 (2013).

[67] L. Savary, K. A. Ross, B. D. Gaulin, J. P. C. Ruff, and L. Balents, Order by Quantum Disorder in $Er_2Ti_2O_7$, Phys. Rev. Lett. **109**, 167201 (2012).

[68] J. Lago, I. Živković, B. Z. Malkin, J. Rodriguez Fernandez, P. Ghigna, P. Dalmas de Réotier, A. Yaouanc, and T. Rojo, $CdEr_2Se_4$: A New Erbium Spin Ice System in a Spinel Structure, Phys. Rev. Lett. **104**, 247203 (2010).

[69] L. F. Chibotaru and N. Iwahara, Ising exchange interaction in lanthanides and actinides, arXiv:1504.00784 [cond-mat.str-el].

[70] J. M. Baker, Interactions between ions with orbital angular momentum in insulators, Rep. Prog. Phys. **34**, 109 (1971).

[71] A. J. Freeman and J. P. Desclaux, Dirac-Fock studies of some electronic properties of rare-earth ions, J. Magn. Magn. Mater. **12**, 11 (1979).

[72] W. P. Wolf and R. J. Birgeneau, Electric multipole interactions between rare-earth ions, Phys. Rev. **166**, 376 (1968).

[73] R. J. Birgeneau, M. T. Hutchings, J. M. Baker, and J. D. Riley, High-degree electrostatic and exchange interactions in rare-earth compounds, J. Appl. Phys. **40**, 1070–1079 (1969).

[74] G. A. Gehring and K. A. Gehring, Co-operative Jahn-Teller effects, Rep. Prog. Phys. **38**, 1 (1975).

[75] O. Tchernyshyov and G. W. Chern, in *Introduction to Frustrated Magnetism* (Springer, Berlin, 2011), pp. 269–291.